J Mater Sci (2007) 42:2492–2498
DOI 10.1007/s10853-006-0797-x

Characterization of $Ba_{0.9}Sr_{0.1}TiO_3$ prepared by low temperature chloride aqueous synthesis

Srimala Sreekantan · Ahmad Fauzi Mohd Noor · Zainal Arifin Ahmad · Radzali Othman · Anthony West · Derek Sinclair

Received: 13 April 2005 / Accepted: 6 December 2005 / Published online: 12 March 2007

Abstract $Ba_{0.9}Sr_{0.1}TiO_3$ powder was processed at 80°C by reacting Ti sol in aqueous solutions that contained $BaCl_2$, $SrCl_2$ and NaOH at atmospheric pressure. Well-crystallized, spherical, nanosizes powders were formed by this method. The powders were found to have a cubic structure, which was retained even after heating at 900°C. Sintering at 1400°C, led to the formation of a tetragonal structure with a secondary phase of $Ba_6Ti_{17}O_{40}$. Abrupt grain growth was observed at 1400°C. The electrical response of the sample sintered at 1400°C has three electrically different regions. Each region of the sample is represented by different *RC* element. Element 1 (R_1C_1) is the most resistive and its capacitance ishigh (0.5 $nFcm^{-1}$) indicating a thin region, probably the grain boundary. Element 2 (R_2C_2) shows a smaller resistance value compared to element 1. The capacitance value of element 2 is temperature-dependent and displays a Curie–Weiss behaviour, indicative of a ferroelectric material above T_c. The lower capacitance of C_2 (15 $pFcm^{-1}$) indicates that it is a much thicker region than element 1 and can be assigned as a ferroelectric bulk region. Element 3 is probably an electrode effect.

S. Sreekantan (✉) · A. F. M. Noor · Z. A. Ahmad · R. Othman
School of Materials & Mineral Resource Engineering, Universiti Sains Malaysia, Engineering Campus, 14300 Nibong Tebal, Seberang Perai Selatan, Malaysia
e-mail: srimala1974@yahoo.com

A. West · D. Sinclair
Department of Engineering Materials, University of Sheffield, Sir Hadfield Building, Mappin Street, Sheffield S1 3JD, UK

Introduction

Barium titanate (BT) and other perovskite-type electroceramic materials have been the heart and soul of several multibillion dollar electronic industries [1] for more than 50 years due to the high dielectric constant and ferroelectric properties. Since the discovery of ferroelectricity in single-crystal materials (Rochelle salt) in 1921, there has been a continuous progression and technology developments of perovskite-type electroceramic materials. One such material, Sr doped BT known as barium strontium titanate (BST), has been one of the important areas of research in electronic materials over the last few years. The significance of this electroceramic material is mainly due to the wide variety of applications such as in phased array antennas, capacitor–varistor protection devices for microelectronic circuit [2] and uncooled pyroelectric IRFPA (infrared focal plane arrays) for low cost IR imaging [3, 4]. BST are also used extensively in integrated circuit (IC) capacitors and in dynamic random access memory (DRAM) cells [5–7] due to the high electrical charge storage capacities. Recently, BST films were used in the formation of graded ferroelectric devices (GFD's) [8]. The performance parameters in these devices are highly dependent on the physical and chemical characteristics, namely, stoichiometry,

homogeneity, phase purity, particle size and the distribution of the starting BST powders. To achieve the desired characteristics, several wet chemical methods, e.g. sol–gel, co-precipitation and hydrothermal were tried for the synthesis of fine BST powders with better reproducibility and quality [9–15] at lower temperatures. In a wet chemical method, temperature and pressure are two factors that have critical influences on the structure and property of the products. A higher temperature and pressure may improve the crystallinity of the fine powders but can lead to a higher level of processing inconveniences and difficulties in the size control of the products. Continuous effort is found in the literature to develop techniques for making high-quality powders at lower temperatures and under ambient pressure. As an example, the crystallization of BT via a conventional solid-state reaction requires a calcinations temperature >1000°C but the synthesis temperature via a chemical method (such as the hydrothermal method) can be as low as 100–280°C [16–20]. There seems to be a lot of attention still focused in lowering the synthesis temperature and pressure. Wada et al. have developed a method called a low-temperature direct synthesis (LTDS) and has been proposed for the synthesis of BT nanoparticles [21] but the particles formed in this experiment were not uniform in terms of size and shape, and tend to be aggregated. Gherardi and Matijevic [22] successfully prepared spherical colloidal (submicron size) BT particles of a narrow size distribution by homogeneous precipitation involving a relatively expensive titanium alkoxide. Recently, Cho and Kuwabara [23] reported the synthesis of partially crystallized BT xerogels with different nano-crystalline structure from a high concentration sol–gel method. In the present study, BST powder which was prepared by a simple chloride aqueous method at low temperatures, even lower than the boiling point of water at atmospheric pressure, is reported. The chloride aqueous method was established to produce BST by reacting titania sol in alkaline aqueous solutions of $BaCl_2$, $SrCl_2$ and NaOH. As shown in this paper, the chloride aqueous method can results in nanosized, crystalline particles with the formation of a metastable BST phase under certain condition. Furthermore, there have been very little effort to study and characterize the electrical properties of sintered ceramics prepared by chemical methods. Therefore, another aspect of the present investigation is to evaluate the electrical properties of a sintered ceramic using ac impedance spectroscopy, a valuable technique which can distinguish between the different regions (grain boundary, grain core, surface, electrode response, etc.) of the material [24]. In this technique, ac impedance measurements were made over a wide range of frequencies and the different regions of the material were characterized by a resistance and capacitance, usually placed in parallel. The characteristic relaxation time or time constant, τ, of each RC element is given by the product of R and C (Eq. 1).

$$\tau = RC \tag{1}$$

$$\omega_{\max} RC = 1 \tag{2}$$

In the frequency domain, RC elements are separable due to the relation shown in Eq. 2, which holds at the frequency of maximum loss, $\omega_{\max}$, in the impedance spectrum. Based on the impedance spectrum, it is therefore usually possible to identify different RC elements and assign them to appropriate regions of the sample. The values of the individual R and C element may be quantified. In general, data obtained by impedance spectroscopy was analysed in terms of four possible formalisms, the impedance (Z^*), the electric modulus (M^*), the admittance (Y^*) and permittivity ϵ^*. These are interrelated [25, 26]:

$$M* = j\omega C_o Z* \tag{3}$$

$$\varepsilon* = (M*)^{-1} \tag{4}$$

$$Y = (Z*)^{-1} \tag{5}$$

$$Y = J\omega C_o \varepsilon* \tag{6}$$

where ω is the angular frequency, $2\pi f$ and C_o are the vacuum capacitance of the measuring cell and electrodes with an air gap in place of the sample.

Experimental procedure

Titanium butoxide [$Ti(OBu)_4$] (99% Fluka Chemical Co.) was used as a precursor and butanol [BuOH] (99.9% J.T. Baker) as a solvent. Nitric acid (HNO_3) (Merck) was used as the peptizing agent. All reagents and solvents were used in as-received forms, without any purification. Titania precipitation was obtained by adding 0.4 M of the titanium butoxide into distilled water. The mixture was stirred at a high speed (300 rpm) whilst the titanium butoxide was added drop-wise. The amount of water was fixed at a [H_2O]/[Ti] molar ratio (r) of 110. In a previous paper [27], the effect of r ratio on titania particle formation had been studied in details. The precipitates were washed with distilled water four times using a centrifuge. Subsequently, the peptization reaction was initiated by

further addition of dilute HNO_3 ([HNO_3] = 0.25 M) in a reaction vessel and placed in a temperature control bath at 60°C. During peptization, the milky dispersion (titanium oxy-hydroxide) changed to a clear light-blue solution, which is indicative of the resuspension of the precipitates and the reduction of the particle size. Simultaneously, alkaline aqueous solutions that contained barium and strontium were prepared by initially boiling distilled water for at least 30 min to remove dissolved CO_2. The water was maintained at a temperature of 80°C under moderate stirring while appropriate amounts of $BaCl_2 \cdot 2H_2O$ (Merck, 99%), $SrCl_2 \cdot 6H_2O$ (Merck, 99%) and 1 M NaOH (Merck, 99.9%) were added. In this case, 0.9 mol $BaCl_2$, 0.1 mol $SrCl_2$ and 1 mol NaOH were used to prepare $Ba_{0.9}Sr_{0.1}TiO_3$. After the starting chemicals were dissolved, the solutions were filtered using a Buchner funnel. The filtered solution was kept in polyethylene bottles. After purging and backfilling with argon, the polyethylene bottles were sealed and stored in an oven at a temperature of 80°C. $Ba_{0.9}Sr_{0.1}TiO_3$ was synthesized by dripping slowly the 1 mole titania sol as described previously, to the solution that was kept in the oven. The initial ratio of barium and strontium in solution relative to titanium was 1. After mixing the titania sol into the solution, the bottles were back-filled with argon, sealed and placed in an oven for reaction. The bottles were then removed from the oven and excess solution was decanted. The powders were washed several times with distilled water that was adjusted to pH 10 using NH_4OH to remove residual barium and strontium cations. The BST powders produced were then placed in petri dishes and dried in an oven at a temperature of 80°C for 24 h. After drying, the powders were uniaxially pressed into pellets at about 100 MPa and sintered at 1400°C for 2 h.

The microstructure was observed using a JEOL JSM 6400 scanning electron microscope with a 20 kV accelerating voltage. Phase identification was performed by high-resolution X-ray diffraction using a Stoe transmission powder diffractometer system (Stoe STADI P) operated at 40 kV and 40 mA. The electrical behaviour of the sintered pellets, which had been electroded with platinum paste and had platinum wire contacts attached prior to use, was measured using a Hewlett Packard 4192A impedance analyzer. Measurements were done over a frequency range of 5 Hz–13 MHz. The temperature of measurement was varied from room temperature to 800°C at an interval of 50°C. All the data measured using ac impedance was corrected for sample geometry. The geometric factor (GF) of the sample was calculated according to Eq. 7:

$$GF = l/A \tag{7}$$

where l is the thickness of the sample (cm) and A is the cross-sectional area (cm^2). This enables the instrument software to give the output in resistivity (ohm cm) rather than resistance value. The term capacitance (F) has been used sometimes although more rigorously this should be termed geometric capacitance (Fcm^{-1}).

Results and discussion

Figure 1a shows the XRD pattern of $Ba_{0.9}Sr_{0.1}TiO_3$ synthesized at 80°C for 48 h. Except for one small peak appearing at about 24°, all the other peaks in the pattern fit with the cubic phase $BaTiO_3$ (space group Pm 3 m) but are shifted slightly to higher angles due to strontium addition. The lattice parameter is $a = c = 4.0150$ Å. The peak sharpness and intensity indicate that $Ba_{0.9}Sr_{0.1}TiO_3$ is well-crystallized. The peak at 24° in the XRD pattern is identified as barium carbonate. The formation of barium carbonate is believed to be a result of the reaction between carbon dioxide that dissolved into the solutions from air and reacted with alkaline earth chloride during the process. XRD peaks that correspond to anatase or rutile titania were not detected. However, at this stage the presence of amorphous titania is still questionable. Figure 1b shows XRD patterns of $Ba_{0.9}Sr_{0.1}TiO_3$ treated at 900°C. The result shows the structure is cubic but there was no carbonate contamination. The lattice parameter changed with the heat treatment temperature, whereby at 900°C, the value is 4.0017 Å. The unit cell volume of the sample decreased by about 1.0% when the powders were heat-treated at 900°C. These phenomena suggest that some kind of defects are present in the lattice and the defect concentration decreased when the powders were heat treated at 900°C, causing the unit cell volume of $Ba_{0.9}Sr_{0.1}TiO_3$ to shrink [28].

XRD pattern of $Ba_{0.9}Sr_{0.1}TiO_3$ sintered at 1400°C for 2 h is shown in Fig. 2. There is a peak splitting of 002/200, 201/210, 112/211 which indicates that the structure transforms to a tetragonal phase (space group P4mm). The lattice parameter for $Ba_{0.9}Sr_{0.1}TiO_3$ sintered at 1400°C is $a = 3.9810$ and $c = 4.0096$ (Table 1). Additionally, a small amount of monoclinic $Ba_6Ti_{17}O_{40}$ (space group A2/a) tends to appear in the sintered sample. The formation of the Ti-rich phase in the sintered ceramic can be related to the high solubility of Ba and Sr in water as compared to Ti [29, 30]. The formation of the perovskite involves the reaction of the Ti with Ba and Sr ions left in solution and this reaction is mainly determined by the effective Ba and Sr

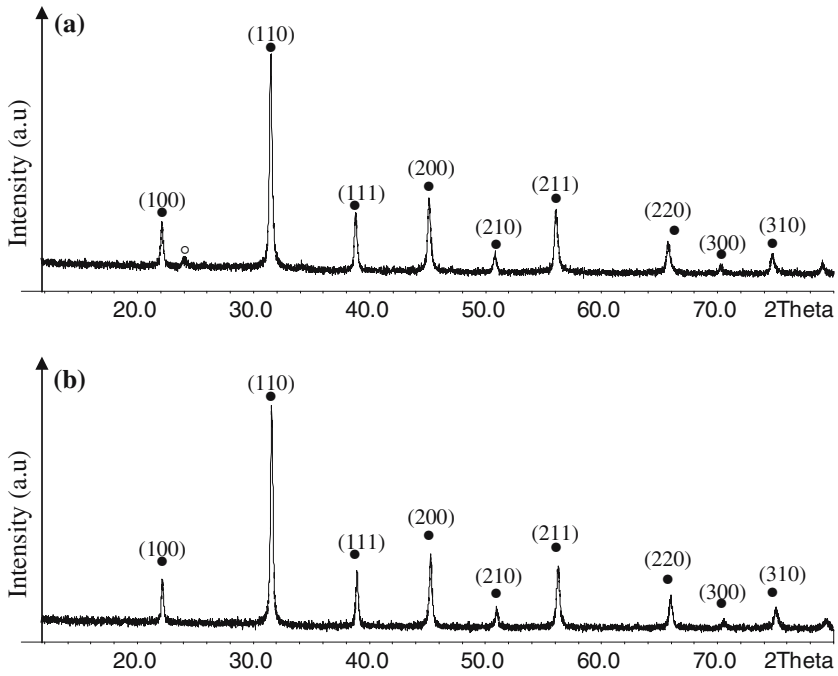

Fig. 1 XRD patterns of $Ba_{0.9}Sr_{0.1}TiO_3$ at different temperatures (**a**) 80°C and (**b**) 900°C. (•) BT-cubic (○) carbonate

concentration in the aqueous phase. When the reaction is incomplete, the powder obtained upon precipitation contained some residual Ti-rich amorphous phase and consequently (Ba + Sr)/Ti < 1. The excess of titanium leads to the formation of a second compound, $BaTi_2O_5$ or $Ba_6Ti_{17}O_{40}$, depending on the temperature of thermal treatment. Therefore, control of (Ba + Sr)/Ti ratio is essential to obtain a single-phase BST powders. More details will be reported in the future.

The crystallite size of the fine particles (synthesized powders) was estimated from the diffraction peak of the (111) plane and the full width of half-maximum by the Scherrer equation. The size of the large particles (sintered sample) was measured under a scanning electron microscope. The crystallite size of the powder prepared at 80°C for $Ba_{0.9}Sr_{0.1}TiO_3$ is 45 nm. The crystallite size was reasonably stable after heat treatment at 900°C and is higher by 15 nm compared to the powder prepared at 80°C (Table 1). However, at 1400°C, there is a drastic increase in the grain size (~50 um). The grains have grown exceptionally large and there is a crystal growth step on the surface (Fig. 3). The abrupt grain growth is believed to be closely related to the formation of a

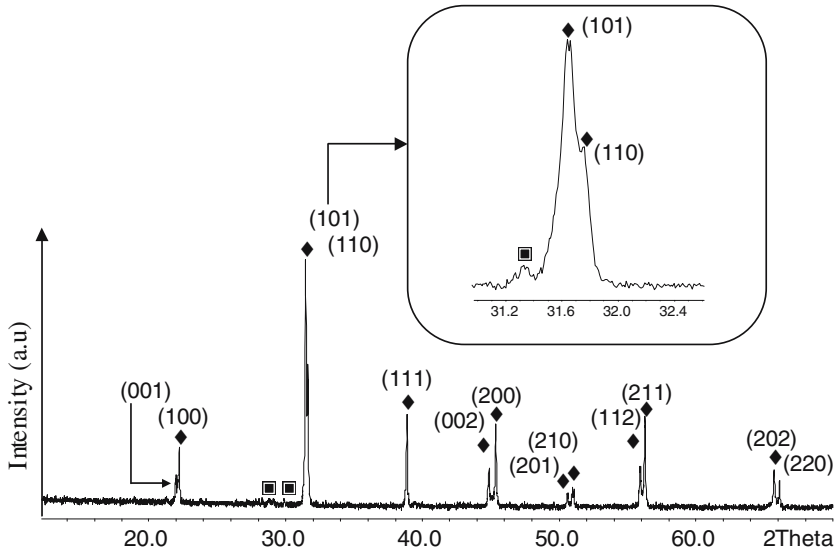

Fig. 2 XRD patterns of $Ba_{0.9}Sr_{0.1}TiO_3$ at 1400°C. (♦) BT-tetragonal, (▣) B_6T_{17}-monoclinic

Table 1 Unit cell parameter and crystallite size of $Ba_{0.9}Sr_{0.1}TiO_3$ at different temperatures

Sintering temperature (°C)	Unit cell parameter				Crystallite size (nm)
	a/Å	*c*/Å	*c*/*a*	*V*/Å^3	
80	4.0150	4.0150	1.0000	64.73	45
900	4.0017	4.0017	1.0000	64.08	59
1400	3.9810	4.0096	1.0072	63.55	—

liquid phase which might have been originated from a Ti-rich phase [31–33]. It should be recalled that there exists a eutectic reaction at 1332°C for the $BaTiO_3$–TiO_2 system [34] which is believed to cause the abrupt grain growth at 1400°C for these respective systems.

Impedance measurement of the sample sintered at 1400°C for 2 h was done from room temperature to 800°C on the heating cycle. A typical impedance complex plane plot, Z^* (Z'' vs. Z'), is shown in Fig. 4. Three different regions can be observed in the impedance complex plane. The big semicircle (R_1C_1) with capacitance 0.5 nFcm^{-1} at the maximum of the impedance semicircle may be assigned to a grain boundary response. When the high frequency plot was enlarged, a small not-well resolved semicircle (R_2C_2) was observed as shown in the insert of Fig. 4. This semicircle may be assigned to a bulk response since the associated capacitance is about 15 pFcm^{-1}. Besides the bulk and grain boundary responses, an electrode response appears at the low frequencies. It is hard to get detail information for this response directly due to the poor resolution.

Voltage dependence work has been carried out in order to ensure that the response observed in the impedance plot (R_1 and R_2) belongs to the bulk or grain boundary effects. Impedance was measured at 510°C with different voltages (0 V, 4 V and 8 V). Biased measurements can cause local heating in the sample which can strongly affect the impedance response; hence the sample was given 15 min cooling time between each measurement. Figure 5 shows the resistance R_1 is dependent on the applied field and R_2 is independent of the applied field. A decrease in R_1 would be expected for a Schottky barrier mechanism at the grain boundaries, whereby the barrier height decreased with increasing applied field. Based on these results, it can be inferred that R_1 response is associated with a grain boundary.

The admittance spectrum which represents the conducting properties of the sample is shown in Fig. 6. The plot consists of two plateaus and the value of the low frequency plateau equals to $1/(R_{gb} + R_b)$; R_{gb} and R_b represent the resistance of the grain boundary and bulk, respectively. As $R_{gb} >> R_b$, the value of the low frequency plateau is approximately equal to the grain boundary conductivity, σ_{gb}. Commonly, the expression for the value of the high frequency plateau is complex. Here, as $R_{gb} >> R_b$ and $C_{gb} >> C_b$, it can be deduced that the value of the high frequency plateau is approximately equal to the bulk conductivity, σ_b [26]. The values of R_{gb} and R_b taken from Fig. 6 are 5.13×10^4 Ωcm and 3.95×10^3 Ωcm, respectively. The resistance is rather low although it is fired in air because alkaline earth titanates are likely to become slightly reduced during sintering [35]. In particular, the reduction of Ti^{4+} to Ti^{3+} provides free electrons for electrical conduction. High sintering temperature (1400°C) may therefore render slightly reduced ceramics, which should exhibit enhanced conductivity and low resistivity. Conductivity data for R_{gb} and R_b at various temperatures are presented as Arrhenius plots in Fig. 7 and have activation energies of 1.07 eV and 0.60 eV, respectively. This implies that an extrinsic conduction mechanism is also active in this material [36].

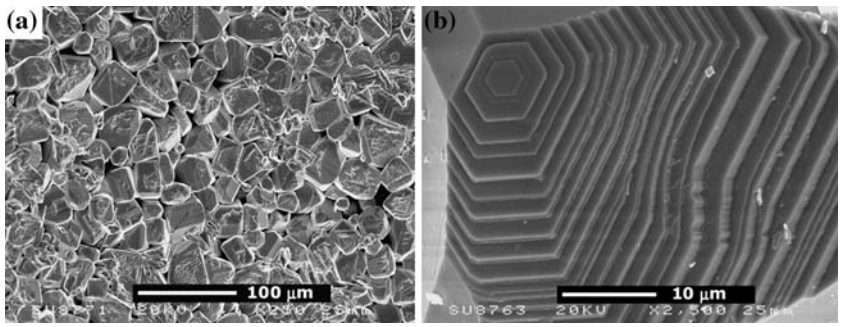

Fig. 3 SEM micrographs of as-sintered surfaces at 1400°C with different magnifications (**a**) 250× (**b**) 2500×

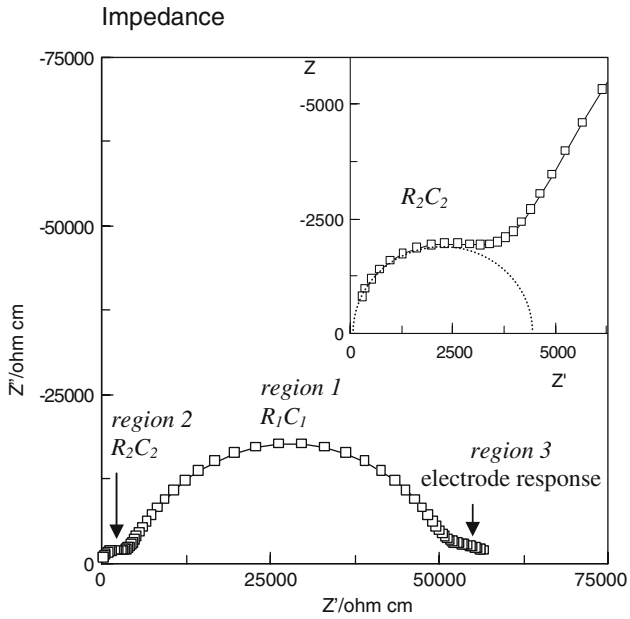

Fig. 4 Complex impedance plot of $Ba_{0.9}Sr_{0.1}TiO_3$ at 535°C

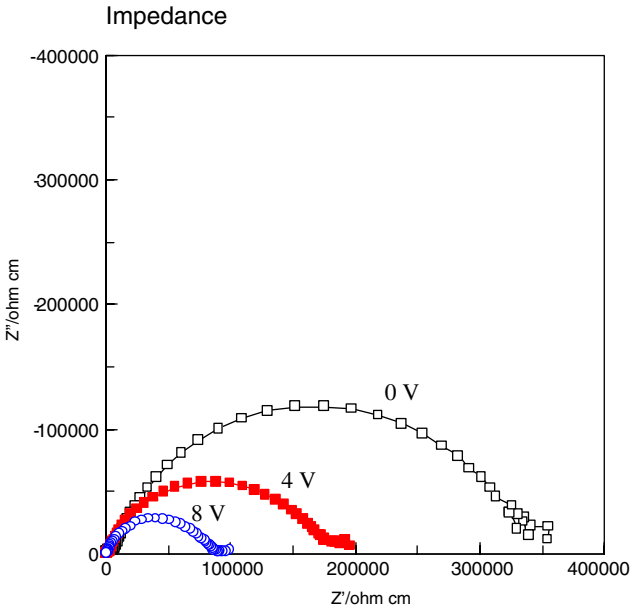

Fig. 5 Applied field-dependent resistance for R_1 element

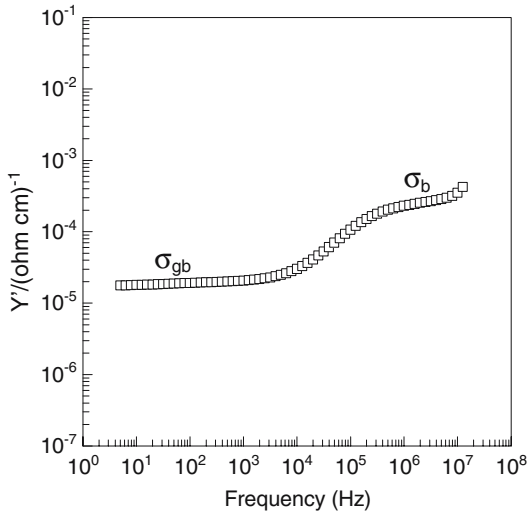

Fig. 6 Admittance spectrum at 535°C

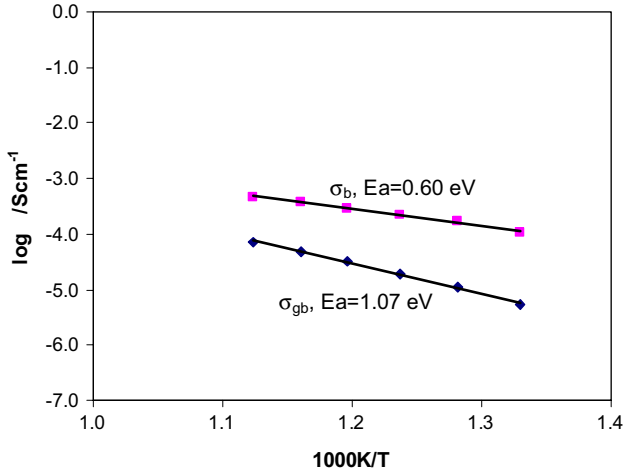

Fig. 7 Arrhenius plots of the bulk and grain boundary conductivities

The capacitance data as a function of temperature for the high frequency plateau of C vs. log f plot is shown in Fig. 8a. The value of this plateau is assigned to capacitance of the bulk, C_2. The data shows C_2 rises with temperature up to the Curie point (~80°C), after which further increase in temperature causes a decrease in C_2. Curie–Weiss behaviour is confirmed by plotting the reciprocal capacitance against temperature (Fig. 8b). A linear plot extrapolating to the Curie point is obtained. Curie–Weiss behaviour exhibited by C_2 is characteristic of the bulk response of a ferroelectric material above its Curie point. Unfortunately, at low temperature, no grain boundary plateau appears because the bulk capacitance rises rapidly as the temperature approaches the Curie point and therefore the Curie–Weiss behaviour exhibited by C_1 is difficult to be determined. However, the large capacitance value (~0.5 nFcm^{-1}) indicates that C_1 is attributed to the grain boundary and this region is thin.

Conclusion

Nanosize (45 nm), well-crystalline cubic phase was successfully obtained at 80°C via a chloride aqueous method. The characteristics of the powder in terms

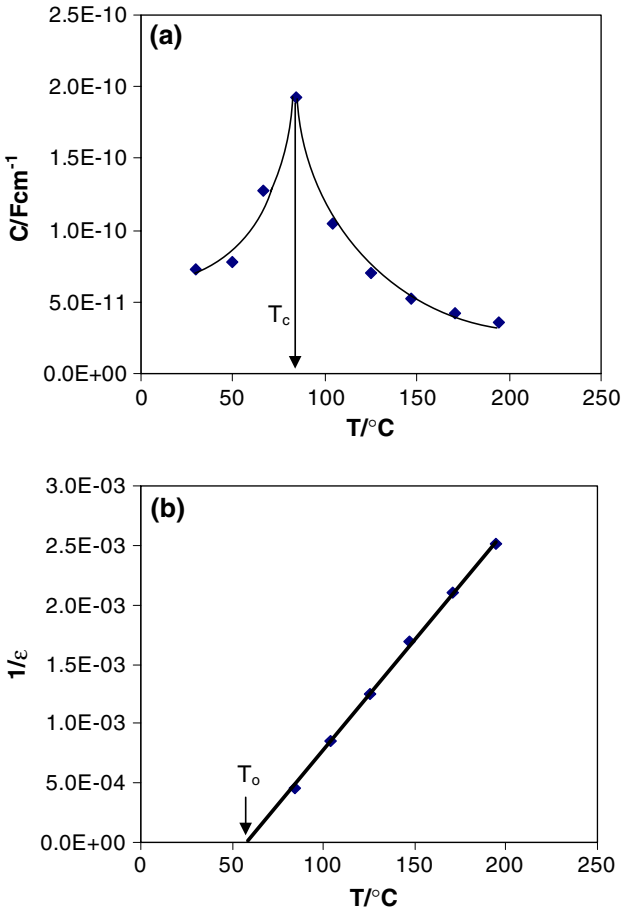

Fig. 8 (**a**) Temperature-dependent capacitance for C_2 element (**b**) Curie–Weiss plot for C_2 element

of crystallite size, morphology and phase were still retained till 900°C. At 1400°C, the structure was tetragonal and a massive grain growth was observed. The electrical characterization shows three electrically different regions. Element 1 (R_1C_1) is a grain boundary, element 2 (R_2C_2) is a ferroelectric bulk region and element 3 is an electrode effect.

References

1. Haertling GH (1999) J Am Ceram Soc 82:797
2. Sengupta LC, Ngo E, O'Day ME, Laccto R (1995) Proc. 1994 IEEE 13th Int. Symp. 622
3. Zhang T, Ni H (2002) Sensor Actuator A 100:252
4. Whatmore RW (1991) Ferroelectrics 118:241
5. Khan M, Burks DP, Burn I, Schulze WA (1988) In: Levinson LM (ed) Electronic ceramics. Marcel Dekker, New York, p. 191
6. Qutzourhit A, Trefny JU, Kito T, Yarar B, Naziripour A, Hermann AM (1995) Thin Solid Films 259:218
7. Dietz GW, Schumacher M, Waser R, Streiffer SK, Basceri C, Kingon AI (1997) J Appl Phys 82:2359
8. Jeon JH, Hahn YD, Kim HD (2001) J Euro Ceram Soc 21:1653
9. Komarneni S, Li QH, Stefansson KM, Roy R (1993) J Mater Res 8:3176
10. Gallagher PK, Schrey F, DiMarcello FV (1963) J Am Ceram Soc 46:350
11. Schrey F (1965) J Am Ceram Soc 48:401
12. Selvam IP, Kumar V (2002) Mater Lett 56:1089
13. Thakur OP, Prakash C, Agrawal DK (2002) Mater Lett 56:970
14. Roeder RK, Slamovich EB (1999) J Am Ceram Soc 82:1665
15. Khollam YB, Bhoraskar SV, Deshpande SB, Potdar HS, Pavaskar NR, Sainkar SR, Date SK (2003) Mater Lett 57:1871
16. Urban JJ, Yun WS, Gu Q, Park HK (2002) J Am Chem Soc 124:1186
17. O'Brien S, Brus L, Murray CB (2001) J Am Chem Soc 123:12085
18. Hernandez BA, Chang KS, Fisher ER, Dorhout PK (2002) Chem Mater 14:480
19. Perez-Maqueda LA, Dianez MJ, Gotor FJ, Sayagues MJ, Real C, Criado JM (2003) J Mater Chem 13:2234
20. Urban JJ, Spanier JE, Ouyang L, Yun WS, Park HK (2003) Adv Mater 15:423
21. Wada S, Tsurumi T, Chikamori H, Noma T, Suzuki T (2001) J Crystal Growth 229:433
22. Gherardi P, Matijevic E (1988) Colloids Surf 32:257
23. Cho JH, Kuwabara M (2004) J Euro Ceram Soc 24:2959
24. Irvine JTS, Sinclair DC, West AR (1990) Adv Mater 2:132
25. Sinclair DC, Finlay DM, West AR (2000) Int Ceram 2:33
26. Sinclair DC, West AR (1989) J Appl Phys 66:3850
27. Srimala S., Ahmad Fauzi MN, Zainal Arifin A, Radzali O (2004) JIMM 5:33
28. Xia CT, Shi EW, Zhong WZ, Guo JK (1995) J Euro Ceram Soc 15:1171
29. Moon J, Suvaci E, Li T, Costantino SA, Adair JH (2002) J Euro Ceram Soc 22:809
30. Testino A, Buscaglia MT, Viviani M, Buscaglia V, Nanni P (2004) J Am Ceram Soc 87:79
31. Lee SB, Sigle W, Ruhle M (2002) Acta Mater 50:2151
32. Henning DFK, Janssen R, Reynen PJL (1987) J Am Ceram Soc 70:23
33. Rios PR, Yamamoto T, Kondo T, Sakuma T (1998) Acta Mater 46:1617
34. Lee BK, Chung SY, Kang SJL (2000) J Am Ceram Soc 83:2858
35. Morrison FD, Sinclair DC, Skakle JMS, West AR (1998) J Am Ceram Soc 81:1957
36. West AR (1984) Solid state chemistry and applications. John Wiley & Sons, Chichester, p. 281